nzsee
NEW ZEALAND SOCIETY FOR EARTHQUAKE ENGINEERING

Study on floor-slab out-of-plane effect of a 2-storey low-damage concrete wall building

A. Gu, G.W. Rodgers
University of Canterbury, Christchurch.

Q. Yang, R.S. Henry
University of Auckland, Auckland.

Y. Lu, Y. Zhou
Tongji University, China.

ABSTRACT

In 2019, a system-level shake-table test of a 2-storey low-damage concrete wall building was conducted using the multi-functional shake-table array at Tongji University as part of an international collaborative project between QuakeCoRE and ILEE. Test results of the low-damage concrete wall building showed an over-strength of the test building where the observed experimental strength exceeded that expected from design. This over-strength factor was largely attributed to the floor-slab out-of-plane effect resulting from the coupled wall-to-floor connection in the long-span direction. Preliminary simulation results of the test building planar models have also shown a deficiency in predicting the wall building overall strength. Hence, it is necessary to further evaluate the floor slab out-of-plane strength contribution to the test building. In this study, the floor slab deformation induced by the unbonded post-tensioned (UPT) wall in the longitudinal (long-span) direction and beam-slab connection flexural strength are considered as the main sources of the test building over-strength. Floor slab shell element models were established in ABAQUS software to quantify the strength contribution induced by the UPT wall uplift in the longitudinal direction. The beam-slab connection flexural strength was calculated by adopting the plane section assumption. These strength contributions were simplified to lumped rotational springs and included in the planar models at slotted-beam joints. The overturning moments of the modified planar models were increased 11% on average compared with the original planar models, and showed an improved agreement with the test results.

1 INTRODUCTION

In 2019, a low-damage concrete wall building was tested on the multi-functional shake-table array at the Jiading Campus of Tongji University as part of a collaboration project between the International Joint Research Laboratory of Earthquake Engineering (ILEE) and the New Zealand Centre for Earthquake Resilience (QuakeCoRE). The test building consisted of UPT walls as the primary lateral load resisting system and perimeter frames that mainly carried gravity loads. The UPT walls and other structural components and connections were designed with innovative detailing to reduce system interaction and structural damage. However, the floor-slab effect still influences the overall capacity of the UPT wall test building (Henry et al. 2021). The strength enhancement due to the existence of the floor slab was also observed in shaking table tests of a full-scale 4-story precast concrete building which incorporated UPT walls in one direction. (Garvidou et al. 2017a).

Planar models were established in OpenSees for the test building based on the design assumption and measured materials properties. Floor-slab out-of-plane effects were not included in the planar models. The planar models were capable to predict the in-plane response of the UPT wall while underestimation of simulated global responses was founded compared with test results. In previous three-dimensional finite element analysis on a UPT wall test building, the floor slabs were found to influence the strength of the test building along the UPT wall direction (Gavridou et al. 2017b, Watkins et al. 2017). Hence, the discrepancy between planar models without floor slab elements and corresponding experimental results is expected. The objective of this study was to enhance prediction accuracy of the planar models in capturing the actual test building response under the design-based earthquake (DBE) and the maximum considered earthquake (MCE) intensities for unidirectional loading cases. Floor-slab out-of-plane effects were included to the test building planar models based on the floor slab modelling and analysis of the test building dataset (Henry et al. 2020).

2 MODIFICATIONS OF PLANAR FRAME MODELS

2.1 Floor-slab out-of-plane effects analysis

Figure 1 shows the floor slab systems arrangement in the test building. A double-tee floor system and composite floor system were incorporated in Level 1 (L1) and Level 2 (L2), respectively. The L1 double-tee floor slab was arranged along the longitudinal direction (EW direction), while the L2 composite floor slab was arranged along the transverse direction (NS direction). A steel beam along grid line 2 is incorporated in L2 as a secondary beam underneath the composite floor to support the floor slab, as shown in Figure 1b. In the longitudinal direction, a flexible wall-to-floor link slab connection was applied in the L1 floor slab, and the wall was connected to the composite floor directly in Level 2 (L2). Hence, the UPT wall vertical uplift would influence the adjacent floor slab deformation which induce additional overall capacity of the test building. Moreover, beam-slab connection in the out-of-plane direction would rotate simultaneously when the test building displaced along EW direction. Hence, the beam-slab connection along the NS direction would contribute strength to the frames in EW direction as well. To enhance the accuracy of the planar models in the EW direction, the floor-slab out-of-plane effects should be considered. Since isolated wall-to-floor connections were incorporated in test building NS direction, the strength enhancement due to the UPT wall uplift was diminished. However, the strength capacity underestimation of NS planar models indicated the beam-slab connection along the EW direction still contribute strength to the frames in NS direction.

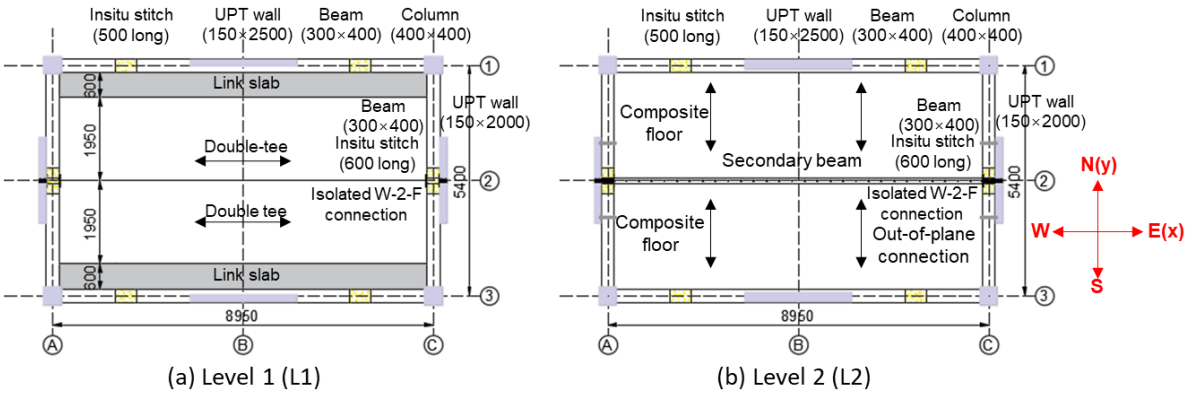

Figure 1: Floor slab systems in each level

2.1.1 Establishment of floor slab models

Finite element models of the floor slab at two levels were established in ABAQUS software, as shown in Figure 2, to evaluate the strength contribution due to wall uplifts in the EW direction. In the floor slab shell element models, the concrete property was represented by concrete damage plasticity behaviour, and plastic behaviour was used for steel properties.

The shell sections of Level 1 and 2 were defined as composite shell sections. The Level 1 and 2 floor slabs were modelled by S4R shell elements with rebar layer. In Level 1 floor slab as shown in Figure 2a, composite shell thickness in the flexible beam-to-floor region was 80 mm and only consists of topping concrete, the shell thickness was 130 mm elsewhere and consists of topping concrete and the Double-Tee flange's concrete. Reinforcement in the floor slab was considered in rebar layer. Double-Tee ribs were modelled by beam elements. The rib ends were constrained to the slab by joint connector, and the ribs at middle were constrained to the slab by beam connector. In Level 2 floor slab as shown in Figure 2b, the composite floor slab was modelled by alternating strips of shell elements denoted strong and weak strips, and the strips were oriented parallel to the ribs in the steel tray (Main 2014). The strong/weak strip has equivalent concrete rectangular sections with 130 mm/70 mm thickness. The steel tray was considered as a 0.8 mm steel layer at the bottom of the equivalent rectangular section with 130 mm. The shell section was represented by composite shell section. The steel beam was modelled by beam elements with steel material property. The steel beam ends and middle nodes were constrained to the slab by joint connector and beam connector, respectively. For level 1 and level 2 floor slab shell element models, floor slab boundary condition was set to be consistent with the boundary condition in the test building. Nodes BA1 and BA3 at the uplifted side of the UPT walls were restrained to an upward loading point.

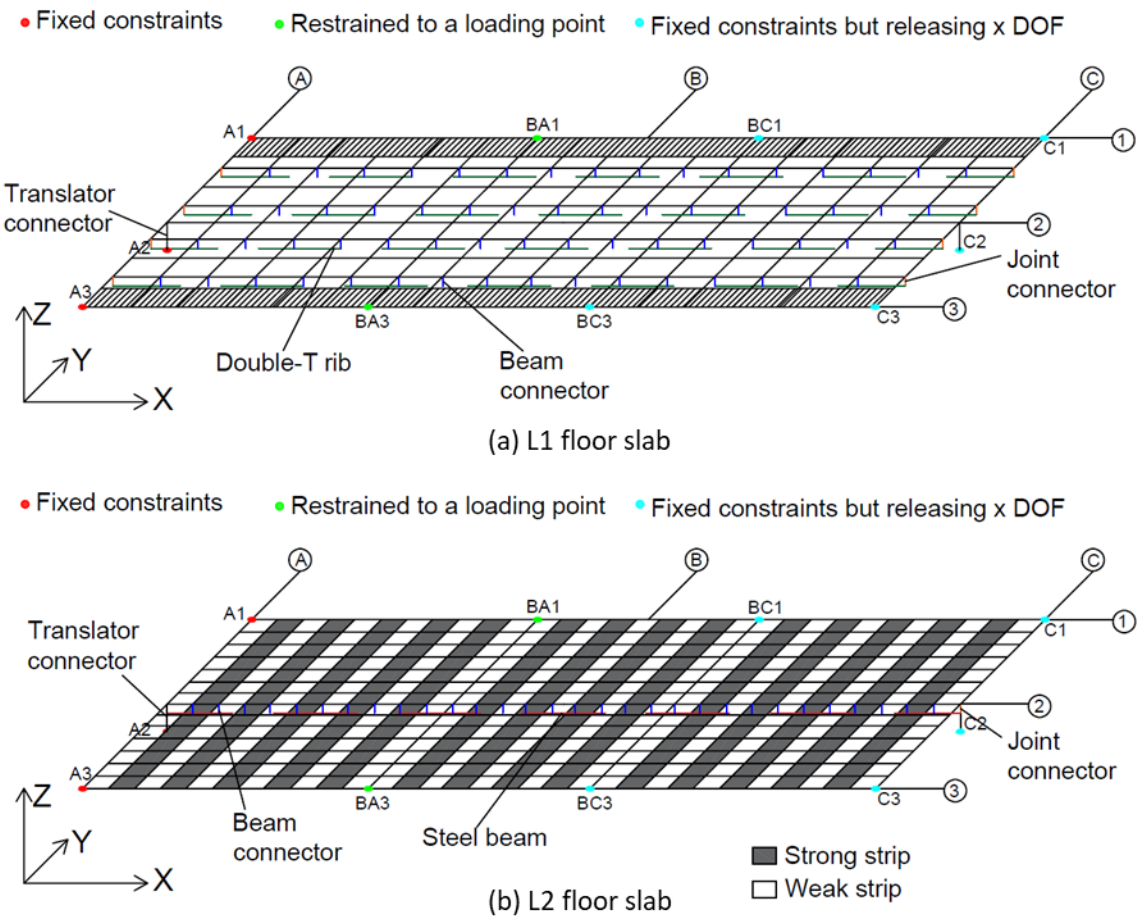

Figure 2: Establishment of floor slab models

The floor slab models simulation results were compared with the measured experimental results under different loading cases. The floor slab vertical displacement measurement arrangements are shown in Figure 3. The floor slab models used in the analysis were validated by the experimental measurements as the models could capture the wall uplift decay at measure points 900mm inwards from the UPT wall which are located on grid lines 1/3. Based on the floor slab shell element models, the strength contributions of the floor slab out-of-plane movement could be obtained. Simplified relationships were also proposed to be adopted in the test building planar models' update. Figure 4 presents a comparison of the results from the ABAQUS model and the simplified relationships.

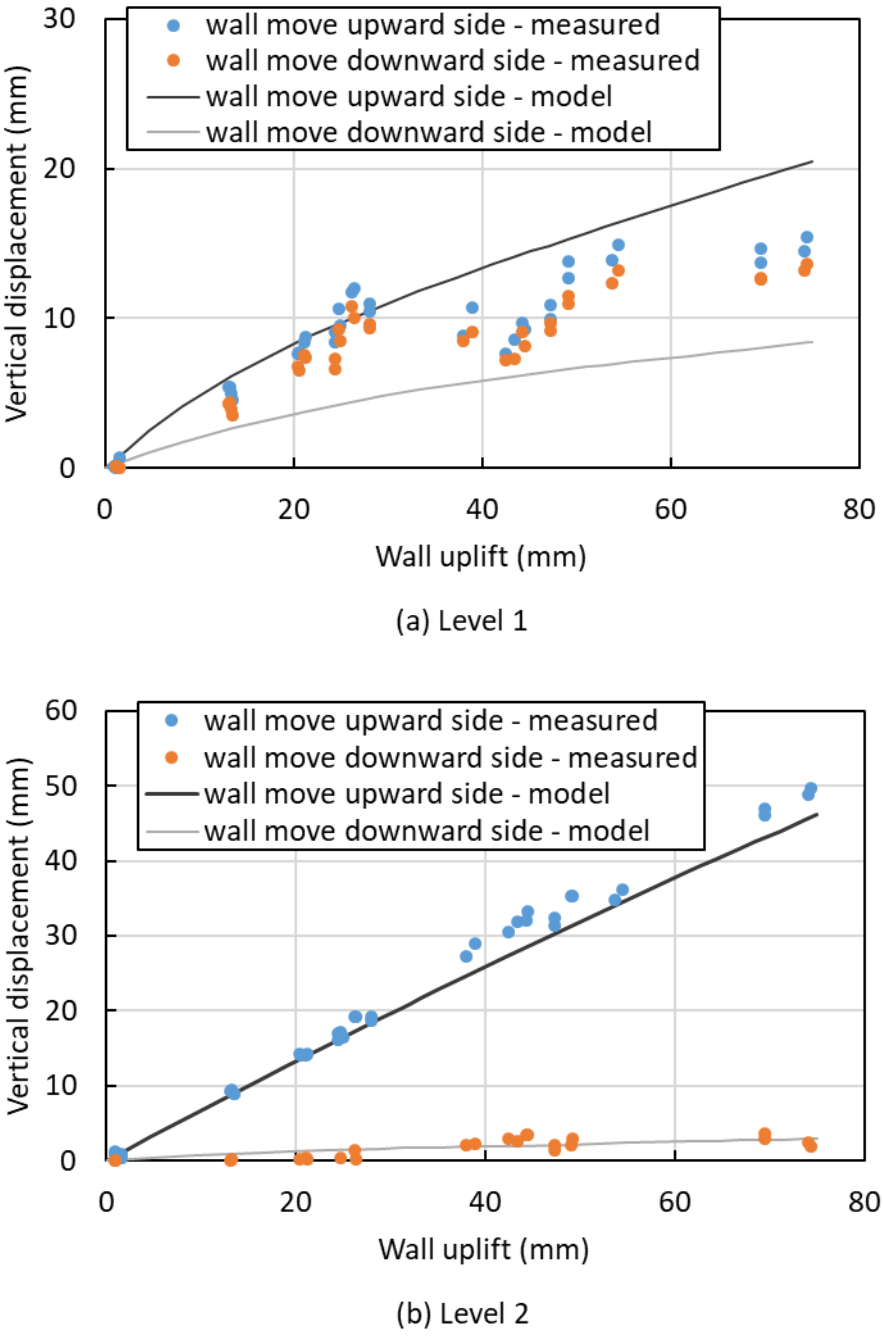

Figure 3: Floor slab vertical displacement comparison between test and simulation results

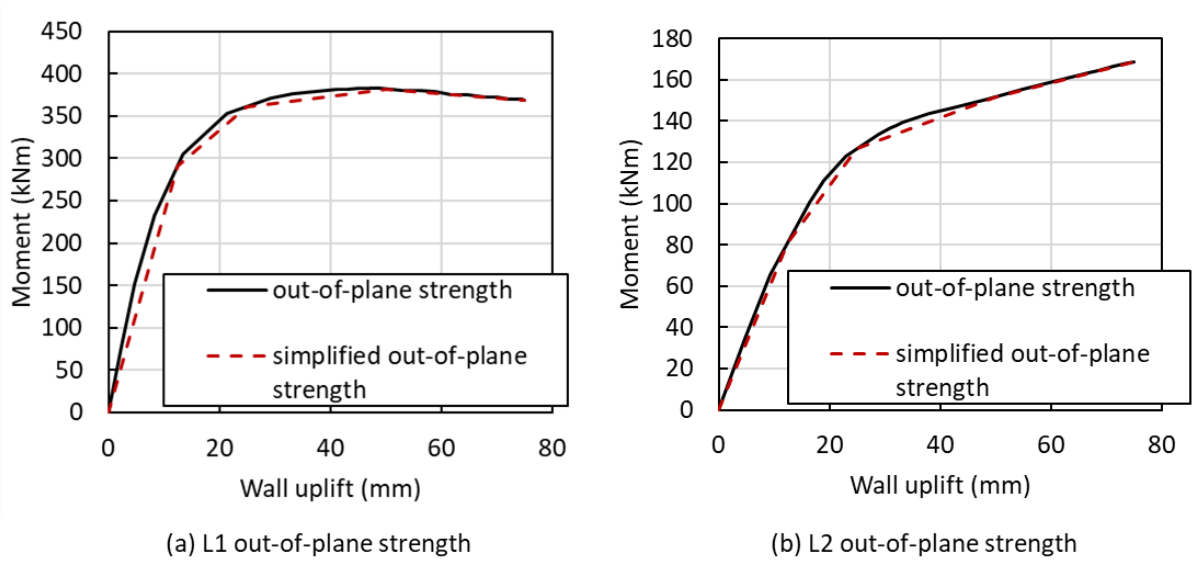

Figure 4: Strength contribution from floor slab out-of-plane movement

2.1.2 Calculations for beam-slab connection strength

The in-plane rotation of the gravity column would generate rotation of the transverse beam and consequently the beam-slab connection would induce a resistant strength (Au 2010). The beam-slab connection strength occurred in both directions of the test building. The plane section assumption was adopted for the beam-slab connection strength calculation. Equation 1-5 presented the beam-slab connection strength at yielding limit state and corresponding rotation calculation for beam-slab connection along grid line 1 at L1. The equivalent compressive concrete region height a could be determined based on the section force equilibrium. A_s represents the total cross area of topping bars along the transverse direction. The yielding stress f_y of the topping bar is 430 MPa for all the beam-slab connections. L_{slab} is the length of the beam-slab connection along grid line 1 at L1. The distance between the centroid of the topping bar and the top surface of beam-slab connection is d_s, and the equivalent thickness of beam-slab connection is $H_{topping}$. The critical length of the of beam-slab connection is two times the strain penetration length of the topping bar $2l_{sp}$ (Pauley and Priestley 1992), l_{sp} should be equal to $0.022f_y d_b$, where d_b represents the diameter of the topping bar reinforcement. The parameter of the equivalent rectangular stress block α, β are 0.85 and 0.8, respectively (ACI 2008). The yielding strain and Young's modulus of topping bar are ε_s and E_s, respectively.

$$a = a' = \frac{A_s f_y}{\alpha f_c L_{slab}} \quad (1)$$

$$M_{b2s,1} = A_s f_y (d_s - \frac{a}{2}) \quad (2)$$

$$\theta_{b2s,1} = \frac{\varepsilon_s}{E_s} 2l_{sp} (d_s - \frac{a}{\beta}) \quad (3)$$

$$M_{b2s,2} = A_s f_y (H_{topping} - d_s - \frac{a'}{2}) \quad (4)$$

$$\theta_{b2s,2} = \frac{\varepsilon_s}{E_s} 2l_{sp} (H_{topping} - d_s - \frac{a'}{\beta}) \quad (5)$$

Table 1 presented the beam-slab connection strength calculation results along each grid. Based on the calculation, the beam-slab connection along Grid 1 L2 would contribute the most to the overall test building strength. It should be noticed that the strength-rotation relationships of beam-slab connection along Grid C

and Grid A are symmetric about the origin, so are the strength-rotation relationships of beam-slab connection along Grid 1 and Grid 3.

Table 1: Calculation for beam-slab connection flexural strength

Beam-slab connection position	A_s (mm^2)	d_s (mm)	L_{slab} (mm)	$H_{topping}$ (mm)	$M_{b2s,1}$* (kN·m)	$M_{b2s,2}$** (kN·m)	$\theta_{b2s,1}$* (rad)	$\theta_{b2s,2}$** (rad)
Along Grid A L1	1099	25	3900	80	23.5	16.4	0.0134	0.0116
Along Grid 1 L1	3375.5	35	8650	80	46.8	61.3	0.009	0.0067
Along Grid A L2	1570	35	5100	70	22.2	22.2	0.0086	0.0086
Along Grid 1 L2	2276.5	45	8650	130***/70	198.9	22.7	0.003	0.0125

*The flexural strength and rotation were corresponding to the situation when the beam rotated clockwise.

**The flexural strength and rotation were corresponding to the situation when the beam rotated counter-clockwise.

***The topping thickness of beam-slab connection along Grid 1 L2 included the depth of rib in the steel stray when the beam rotated clockwise.

2.2 Incorporating floor-slab out-of-plane effect to the original planar models

Because the test building was designed with flexible and isolated floor-to-wall connections to reduce adverse effects of wall and floor interaction, planar frame models were selected to simulate the test building dynamic response in each direction. An accurate simulation of the UPT wall base behaviour and the slotted-beam joints was important for modelling the test building response. For computational efficiency and simulation convenience, the UPT wall bases were simulated using a fiber beam-column element, and elastic beam-column elements were used to model the wall panels that suffered no damage during testing. This modelling method has been verified in prior UPT wall simulation analysis (Watkins et al. 2017). The multi-spring model was proven to capture the mechanical behaviour of slotted-beam joints in component-level experiments (Au 2010). In the multi-spring model, the top concrete hinge region was modelled by macro multiple concrete springs, longitudinal and diagonal hanger reinforcement springs. A modified multi-spring model for slotted-beam joints was proposed for this planar model based on the multi-spring model. The modified multi-spring model was identical with the multi-spring model except that the top hinge regions of the slotted-beam joints were modelled using fiber beam-column elements representing the concrete region and twoNodeLink elements representing the longitudinal and diagonal hanger reinforcement.

The beams and columns in the perimeter frames were modelled using elastic beam-column elements. In the test building, the gravity columns were connected to the foundation by unbonded rebars without any preload applied (Henry et al. 2021). As a result, only minimal moment transfer was possible, so the boundary condition of column bases in the model was assumed to be pinned. Since the beam and column components in the test building suffered little damage, the section moment of inertia for both the beam and column elements were set to be 0.6 I_{gross}. The elastic modulus of the frame concrete was calculated to be $5000\sqrt{f_c'}$ MPa. Truss elements were chosen to represent the PT bars and steel fuses. TwoNodeLink elements were chosen for the HF2V and viscous dampers incorporated in the D1b and D1c configurations. The transverse direction model was similar to that in the longitudinal direction, except for the fact that the UPT wall in the transverse direction was offset from the frame. The isolating wall-to-floor connections were also considered in the transverse direction frame model using zeroLength elements to release the vertical constraints between the UPT wall and beam/floor.

The floor-slab out-of-plane effects due to the UPT wall uplift and beam-slab connection were considered in the planar models by incorporating lumped rotational springs into slotted-beam joints. The beam-slab connection flexural strengths were evenly assigned to the beam-to-column slotted-beam joints in each level. The floor slab out-of-plane strengths induced by UPT wall uplift were also evenly assigned to the beam-to-wall slotted-beam joints in the EW direction. MultiLinearElastic material was adopted to represent the moment-rotation relationships for strength increased by floor-slab out-of-plane effects. The updated planar models were shown in Figure 5. Connection flexibility at wall base was considered in the updated planar models. An elastic material accounted for 1 mm sliding tolerance was connected to the steel fuse material in series for D1a, D1c and D2 design configuration to account for connection flexibility. The elastic displacement of the viscous damper connecting elements was considered by reducing the elastic stiffness parameter in the viscous damper material (Akcelyan, Lignos and Hikino 2018) for D1b design configuration.

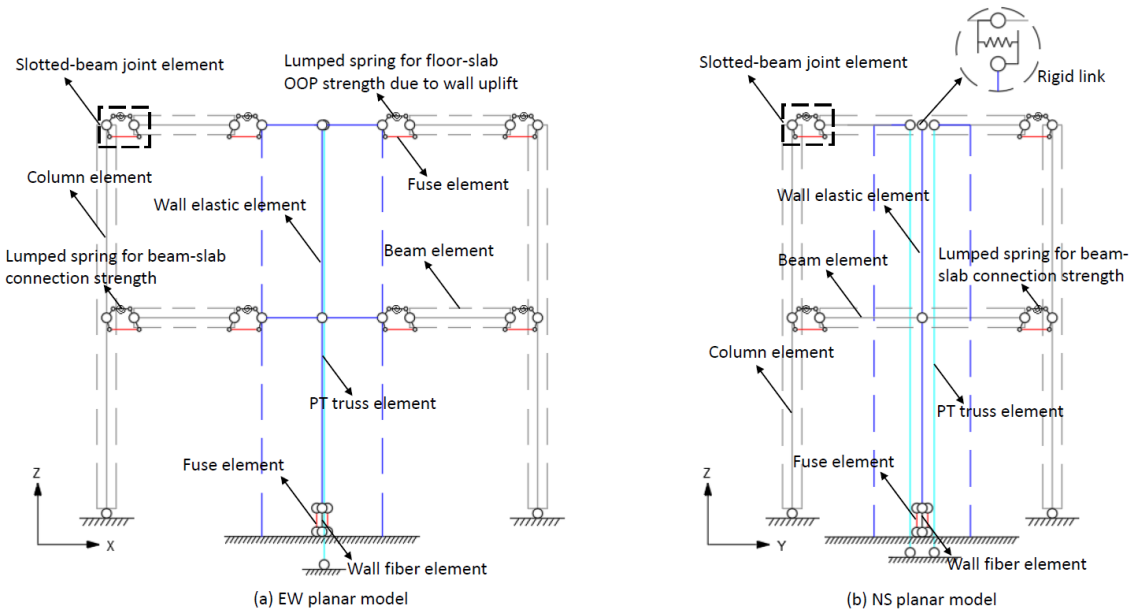

Figure 5: Planar models for D1a design configuration considered the floor-slab out-of-plane effect

3 GLOBAL RESPONSE ANALYSIS

Figure 6 compares the updated planar model global response with the original planar model in the unidirectional loading cases under DBE and MCE intensities. Although the simulation results of the updated planar models still underestimate the global response by 14% for peak roof drift response and 20% for peak base moments on average, the updated planar models gave more accurate peak global responses than the original models for unidirectional loading cases. Comparing to the original planar models, the peak roof drifts were increased for the updated planar models in both direction considering D1 design configuration, the peak roof drifts were decreased slightly in both directions considering D2 design configuration, particularly under MCE intensity. Nevertheless, the peak roof drifts obtained from the updated models were closer to the test results. The peak strength obtained from the updated planar models were much closer to the peak responses from test results, and the peak base moments of the updated planar models were increased 13% and 9% on average for the EW and NS directions, respectively.

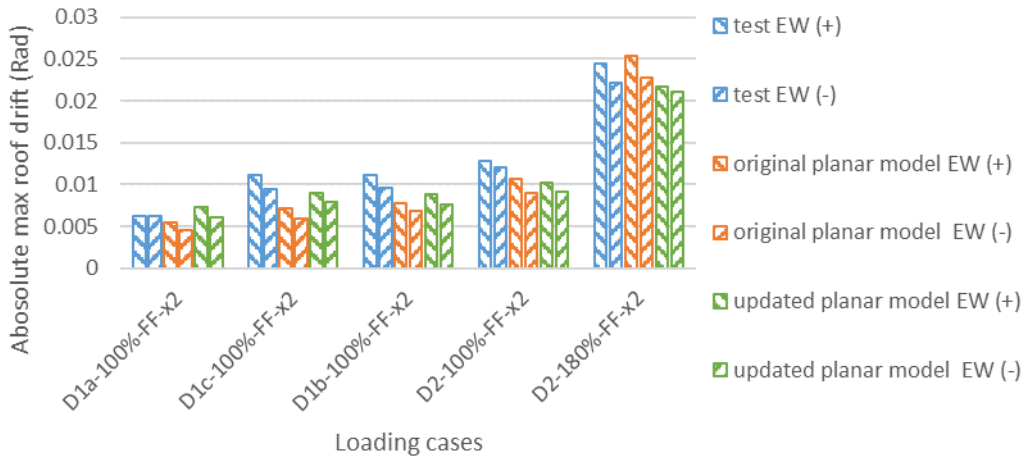

(a) Roof drift in EW direction

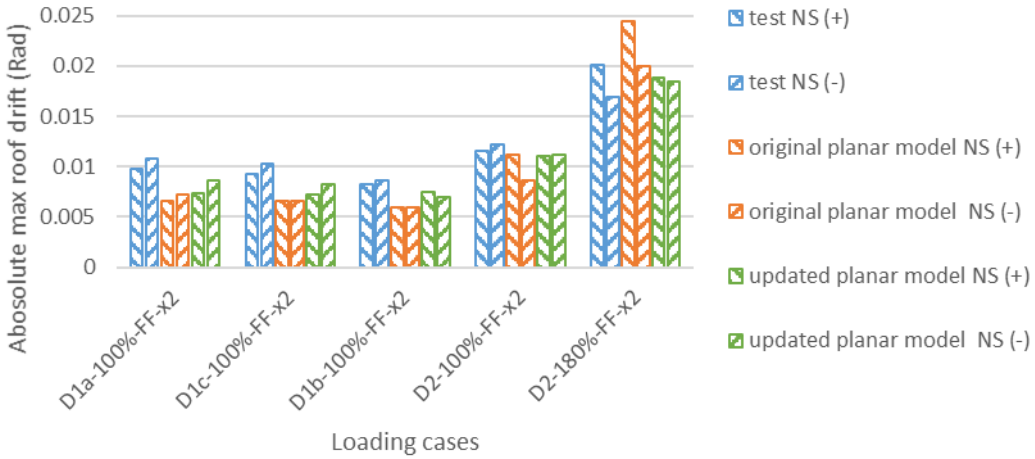

(b) Roof drift in NS direction

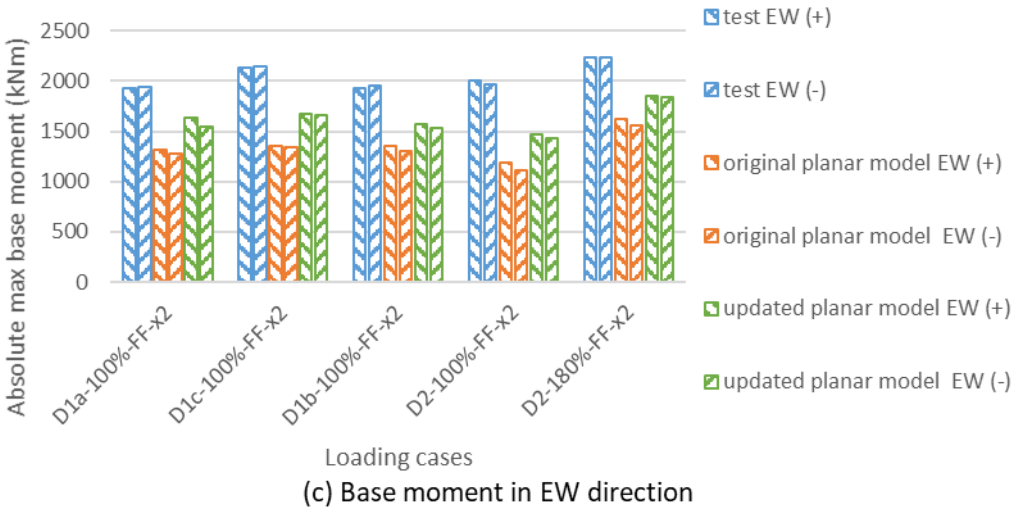

(c) Base moment in EW direction

(d) Base moment in NS direction

Figure 6: Comparisons of peak global responses between planar models and test results

4 CONCLUSION

In this study, an updated model considering the floor-slab out-of-plane effect was proposed to get a more accurate simulated response in unidirectional loading cases under DBE and MCE intensities. The moment contribution from floor-slab out-of-plane effects was first evaluated. Strength contribution due to wall uplifts in EW direction was obtained from floor-slab shell element model in ABAQUS. Beam-slab connection strength was also calculated based on the plane section assumption. The connection flexibility of energy dissipation devices at wall bases were also included in the updated planar model through the use of a 1mm sliding tolerance. Comparing the global response of updated and original planar frame models, the updated planar model predicted the roof drift and base moments better than the original planar models, and the peak base moments were increased 13% and 9% on average for the EW and NS direction, respectively. The comparison between the simulation results and test results has indicated the floor-slab out-of-plane effect would influence the global responses of the test building in unidirectional loading cases.

ACKNOWLEDGEMENT

The authors would like to acknowledge the financial support provided by International Joint Research Laboratory of Earthquake Engineering (Grant No. ILEE-IJRP-P2-P4-2017), and the New Zealand Ministry of Business, Innovation and Employment (MBIE) Building System Performance. This project was also partially supported by a Rutherford Discovery Fellowship and by QuakeCoRE, a New Zealand Tertiary Education Commission-funded Centre. This is QuakeCoRE publication number 0733.

REFERENCES

ACI Committee. 2008. *Building code requirements for structural concrete (ACI 318-08) and commentary*. American Concrete Institute.

Akcelyan, S., Lignos, D. G., & Hikino, T. 2018. Adaptive numerical method algorithms for nonlinear viscous and bilinear oil damper models subjected to dynamic loading. *Soil Dynamics and Earthquake Engineering* 113: 488-502.

Au, E. V. 2010. *The mechanics and design of a non-tearing floor connection using slotted reinforced concrete beams.* Master's Thesis. Christchurch: University of Canterbury. https://ir.canterbury.ac.nz/handle/10092/4949

Gavridou, S., Wallace, J. W., Nagae, T., Matsumori, T., Tahara, K. & Fukuyama K. 2017a. Shake-Table Test of a Full-Scale 4-Story Precast Concrete Building. I: Overview and Experimental Results. *Journal of Structural Engineering* 143(6): 04017034.

Gavridou, S., Wallace, J. W., Nagae, T., Matsumori, T., Tahara, K. & Fukuyama K. 2017b. Shake-Table Test of a Full-Scale 4-Story Precast Concrete Building. II: Analytical Studies. *Journal of Structural Engineering* 143(6): 04017035.

Henry, R. S., Lu, Y., Zhou, Y., Lu, Y., Rodgers, G. W., Gu, A., Elwood, K. J. & Yang, T. 2020. *Dataset on shake table test of a low-damage concrete wall building*. DesignSafe-CI.

Henry, R. S., Zhou, Y., Lu, Y., Rodgers, G. W., Gu A, Yang, Q., Elwood, K. J. & Yang, T. 2021. Shake-Table Test of a 2-storey Low-Damage Concrete Wall Building. *Earthquake engineering & structural dynamics* 51(12): 3160-3183.

Main, J. A. 2014. Composite Floor Systems under Column Loss: Collapse Resistance and Tie Force Requirements. *Journal of Structural Engineering* 140(8): A4014003.

Paulay, T. & Priestley, M. J. 1992. *Seismic Design of reinforced concrete and masonry buildings.* 1992.

Watkins, J., Sritharan, S., Nagae, T. & Henry, R. S. 2017. Computational Modelling of a Four Storey Post-Tensioned Concrete Building Subjected to Shake Table Testing. *Bulletin of the New Zealand Society for Earthquake Engineering* 50(4): 595-607.